Journal of Hazardous Materials 211–212 (2012) 47–54

Contents lists available at ScienceDirect

Journal of Hazardous Materials

journal homepage: www.elsevier.com/locate/jhazmat

Photoelectrochemical performance of multi-layered BiO_x–TiO_2/Ti electrodes for degradation of phenol and production of molecular hydrogen in water

Hyunwoong Park[a,*], Ayoung Bak[a], Yong Yoon Ahn[b], Jina Choi[c], Michael R. Hoffmann[c]

[a] School of Energy Engineering, Kyungpook National University, Daegu 702-701, Republic of Korea
[b] Department of Physics, Kyungpook National University, Daegu 702-701, Republic of Korea
[c] W.M. Keck Laboratories, California Institute of Technology, Pasadena, CA 91125, United States

ARTICLE INFO

Article history:
Received 4 March 2011
Received in revised form 3 May 2011
Accepted 4 May 2011
Available online 26 May 2011

Keywords:
Photoelectrocatalytic
Electrocatalytic
Hybrid
Water treatment
Titania

ABSTRACT

Multi-layered BiO_x–TiO_2 electrodes were used for the oxidation of chemical contaminants coupled with the production of H_2 characterized by a synergistic enhancement. The BiO_x–TiO_2 electrodes were composed of a mixed-metal oxide array involving an under layer of TaO_x–IrO_x, a middle layer of BiO_x–SnO_2, and a top layer of BiO_x–TiO_2 deposited in a series on both sides of Ti foil. Cyclic voltammograms showed that the BiO_x–TiO_2 electrodes had an electrocatalytic activity for oxidation of phenol that was enhanced by 70% under illumination with AM 1.5 light. When the BiO_x–TiO_2 anode was coupled with a stainless steel cathode in a Na_2SO_4 electrolyte with phenol and irradiated with UV light at an applied DC voltage, the anodic phenol oxidation rate and the cathodic H_2 production rates were enhanced by factors of four and three, respectively, as compared to the sum of each light irradiation and direct DC electrolysis. These synergistic effects depend on the specific electrode composition and decrease on TaO_x–IrO_x and BiO_x–SnO_2 anodes in the absence of a top layer of BiO_x–TiO_2. These results indicate that the BiO_x–TiO_2 layer functions as the key photo-electrocatalyst. The heavy doping level of Bi (25 mol%) in TiO_2 increases the electric conductivity of the parent TiO_2.

1. Introduction

As our industrialized society discharges diverse and more recalcitrant aquatic pollutants, electrochemically assisted advanced oxidation process (EAOP) has received more attention as an end-of-pipe remediation tool for water and wastewater [1–4]. The electrochemical oxidation of aqueous organic pollutants is initiated by generating reactive species that are sorbed on or remotely from the employed anode surface [5,6]. Since the electrochemical reaction occurs primarily at the electrode/water interface, the performance of the electrochemical treatment depends not only on the nature of target substrates [7–10] but also on the nature of the anode [9,11–16] and electrolyte [9,10,13].

The anode can be largely divided into oxide type and non-oxide type; the former includes dimensionally stable anodes (DSAs) [5,13] and Sb–SnO_2 [7,9,17–20] while the latter includes Pt, boron-doped diamond (BDD) [12,21,22], stainless steel [11,12], and carbon [11]. Despite equal scientific importance, the former seems more practical and applicable in terms of cost-competitiveness. The anodes also are often divided into active anodes and non-active anodes according to their oxygen evolution potentials [3,12,16]. For example, the active anodes including Pt [14–17,23], IrO_2 [24,25], and RuO_2 [6,9,17,19] produce molecular oxygen (water oxidation) at low potential ranges (low oxygen evolution potential anodes); conversely, the non-active anodes such as PbO_2 [15,19,23,26], Sb–SnO_2 [9,18–20], and BDD [12,21,22] produce the oxygen at high potential ranges (high oxygen evolution potential anodes). Finally, the anodes also can be separated into electrocatalytic anodes and photo-assisted anodes according to operation mechanism. All the aforementioned anodes fall into the former whereas the latter includes ZnO [27], SnO_2 [28], α-Fe_2O_3 [29], $BiVO_4$ [30], WO_3 [31], and TiO_2 [32–37]. Although these photoanodes have good performances for remediating aquatic pollutants, their main drawback is inactivity in the absence of light primarily due to their intrinsic insulating properties.

We have recently studied several different electrocatalytic anodes such as Nb_2O_5 [8], BiO_x–TiO_2 [10,38,39], RuO_2 [9], and Sb–SnO_2 [9]. A comparison between RuO_2 and Sb–SnO_2 indicated that the general electrocatalytic performances of Sb–SnO_2 (non-active anode) for oxidizing various substrates (methylene blue, acid orange 7, and 4-chlorophenol) were much superior to RuO_2 (active anode) in sodium sulfate electrolyte; yet the relative superiority of Sb–SnO_2 disappears when sodium chloride was used as a supporting electrolyte. In the case of BiO_x–TiO_2 mixed oxide anodes, they

* Corresponding author at: School of Energy Engineering, Kyungpook National University, Daegu 702-701, Republic of Korea. Tel.: +82 53 950 7371; fax: +82 53 952 1739.
E-mail address: hwp@knu.ac.kr (H. Park).

0304-3894/$ – see front matter © 2011 Elsevier B.V. All rights reserved.
doi:10.1016/j.jhazmat.2011.05.009

Table 1
Electrode compositions[a] and light-assisted synergistic effects[b] on cell currents (I_{cell}), anodic degradation rates of phenol ($-k_{obs}$), and cathodic hydrogen production rates (H_2).

Electrode[c]	lst coat	2nd coat	3rd coat	4th coat	Synergy		
					I_{cell}	k_{obs}	H_2
A	Ir–27Ta	–	–	–	1.1	1.2	1.5
B	Ir–27Ta	SnO_2–10Bi	–	–	1.0	1.1	1.7
C	Ir–27Ta	SnO_2–10Bi	TiO_2–4Bi	TiO_2–25Bi–25Na	3.1	4.3	3.2
D	Ir–27Ta	SnO_2–10Bi	TiO_2–4Bi	TiO_2–33Bi	4.3	4.3	3.1

[a] Number refers to mol%.
[b] Synergy = PEC/(DC + light).
[c] Electrodes A, B, C and D correspond to Examples C1, C2, 9 and 6 in Ref. [42] and were prepared using similar but simplified methods.

consist of multi-layered metal oxides and thus retains a robust performance as compared to single-layered analogs. In addition, when coupled with stainless steel cathodes and powered by an external photovoltaic array under sunlight, the BiO_x–TiO_2 anodes have been shown to be capable of treating water under continuous-flow conditions along with the simultaneous generation of molecular hydrogen at the cathode [38,39].

We noted that although BiO_x–TiO_2 anodes were originally developed as electrocatalytic anodes that operate in the absence of light by degeneratively doping with Bi in TiO_2, the presence of TiO_2 might make them retain photoelectrocatalytic activity as well [40,41]. If so, the electrochemical performance of BiO_x–TiO_2 can be boosted by light irradiation and applied to water treatment. However, such photo-assisted electrocatalytic operations should be distinguished from the photocatalytic operations of TiO_2 in that commonly used TiO_2 anodes cannot work at all in the absence of light whereas the BiO_x–TiO_2 maintains its electrocatalytic performances irrespective of light irradiation. In this report, we examined several electrocatalyst compositions that were degeneratively doped with Bi in TiO_2 at levels up to 25–33 mol%. In spite of the heavy level of doping, the BiO_x–TiO_2 layer retained its essential photoelectrocatalytic properties and its characteristic metal oxide surface chemistry, which was dominated by surface titanol (>TiOH) functionalities and their >BiOH analogs. The degeneratively doped BiO_x–TiO_2 electrodes were found to be effective for the oxidative degradation of phenol (C_6H_5OH) and the hydrogen evolution at the cathode.

2. Experimental

2.1. Preparation of multi-layered anodes

A Ti foil (0.5 mm thick) was cleansed with SiC paper and coated with a sequence of layer substrates. The most bottom layer coat (first coat) containing Ir and Ta at a mole ratio of Ir:Ta = 0.73:0.27 was deposited to the Ti base and sealed with BiO_x–SnO_2 mixed oxide at a mole ratio of Bi:Sn = 0.1:0.9 (second coat). Then BiO_x–TiO_2 of a mole ratio of Bi:Ti = 0.04:0.96 were deposited as the third coat; finally BiO_x–TiO_2 oxide layers at different mole ratios of Bi:Ti were coated (fourth coat) (see Table 1). Each successive step of coating requires a specific heat treatment regime at different temperatures and durations (525 °C for 1 h, 425 °C for 10 min, 250 °C for 5 h, and 425 °C for 5 h for the first, second, third, and fourth coats, respectively) [42].

2.2. Surface characterizations

Quantitative elemental micro-analyses were conducted with the JEOL 8200 electron microprobe operated at 15 kV and 10 nA in a focused beam mode using the Probe for Windows software. An X-ray photoelectron microscopy (XPS) analysis was made in an M-probe surface spectrometer (VG Instruments) using monochromatic Al K-α X-rays (1486.6 eV). Scanning electron microscopy (SEM) measurements were performed by a field emission scanning electron microscope (Hitachi, S-4800) at an operating voltage of 3 kV. UV–vis diffuse reflectance absorption spectra of electrode samples were recorded with respect to $BaSO_4$ pellet or pure Ti foil (uncoated) with a UV–vis absorption spectrometer (Shimadzu-2450).

2.3. Electrochemical and photoelectrochemical study

A single thin anode with an active area of 50 cm^2 and a stainless steel (SS) cathode (Hastelloy C-22) of equal size faced each other with a separation distance of 2 mm. The anode–cathode couple was immersed in an aqueous electrolyte solution of sodium chloride (1.5 L). The target substrate (phenol, 1 mM) was added to the background electrolyte (pH ~ 5), which was mixed for 30 min with continuous purging of nitrogen or air gas through the solution. A constant cell voltage or current was applied to the electrodes with a DC-power supply (HP 6263B and 6260B). In addition, a collimated bean of UV-light was simultaneously focused on the anode surface that did not face the SS through the quartz window. A 450 W Hg-Xe arc lamp (Oriel) was used as a light source. Light passed through a 10 cm-IR water filter and a cutoff filter ($\lambda > 320$ nm), and then the filtered light was focused onto the reactor. Sample aliquots and headspace gases were withdrawn by a syringe intermittently during illumination and analyzed.

Cyclic voltammograms of BiO_x–TiO_2 electrode were obtained with a potentiostat (Versastat 3-400) that was connected to saturated calomel electrode (SCE, reference electrode) and Pt-gauze (counter electrode) in 0.1 M NaCl with or without 1 mM phenol. To illuminate the BiO_x–TiO_2 electrode, a 150-W Xe-Arc lamp (Ushio 150-MO) equipped with an AM 1.5 air mass filter was employed. Phenol and its reaction intermediates were analyzed by a high performance liquid chromatography (HPLC, Agilent 1100 series) using a C18 column for separation. The eluent was composed of 55% Milli-Q water (0.1 wt% acetic acid) and 45% acetonitrile at a flow rate of 0.7 mL/min. The amounts of H_2 and CO_2 evolved during electrochemical and/or photoelectrochemical reactions were analyzed by the respective GC/TCD and GC/FID (HP 6890N, N_2 carrier) with a molecular sieve column (30 m × 0.32 mm × 12.00 μm).

3. Results and discussion

3.1. Surface characterization of electrodes

Four different compositional variations of the multi-layered BiO_x–TiO_2 anodes were synthesized. The detailed layering of materials is summarized in Table 1. Electrode A was coated with only Ir (73 mol%) and Ta (27 mol%) while electrode B has an additional layer consisting of 10 mol% Bi-doped SnO_2. The third and fourth coatings on B with Bi-doped TiO_2 are represented by electrodes C and D. Each electrode has a different surface morphology. For

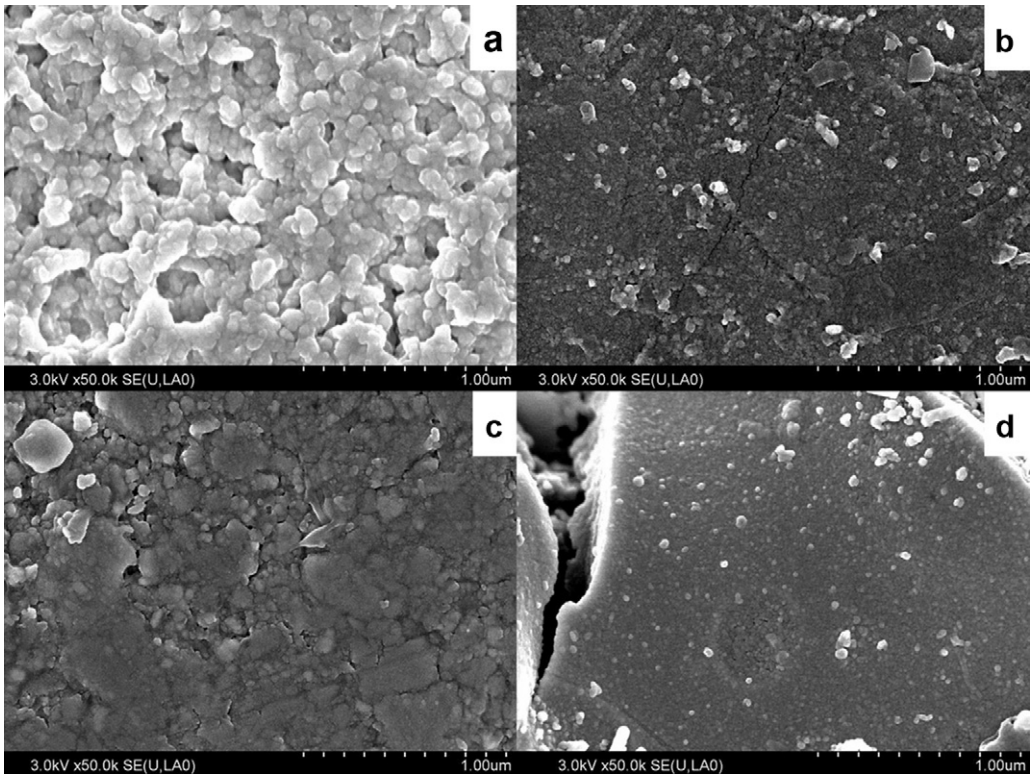

Fig. 1. Scanning electron microscopy images of (a) electrode A, (b) electrode B, (c) electrode C, and (d) electrode D.

example, electrode A has a particle-to-particle connected surface with primary particle size of ca. 100 nm and retains a highly porous structure, while electrode D has a cracked mud-like surface composed of ca. 30 nm-sized particles (Fig. 1). Electrodes B and C have a quite similar surface image with A yet with a more densely packed configuration. Such different surface morphologies, however, might not affect their electrocatalytic and/or photoelectrocatalytic activities. Fig. 2 shows the electron-probe microanalysis (EPMA) data for the cross-sectioned electrode C, the composition of which is Ir–27Ta (first coat), SnO_2–10Bi (second coat), TiO_2–4Bi (third coat), and TiO_2–25Bi–25Na (fourth coat) in series. It was found that the atomic % of iridium and oxygen increase almost linearly along with decreases of Ti-at% up to 6.5 μm in thickness. Sn was found predominately in the coating thickness range of 6.5–8 μm while the Bi-at% increases at 5.6 μm away from the Ti substrate. These results suggest that the layer thicknesses of the first, second, and third/fourth coats are ca. 6.5 μm, 1.5 μm, and 2 μm, respectively. The EPMA results further indicate that in spite of a layer-by-layer application of the successive coatings, those coats are slightly merged into one another during the annealing processes. However, the topmost part is comprised of only Ti, Bi, and O with a minor amount of Sn as confirmed by XPS (Fig. 3). The electrode D also has a similar layer configuration. Finally, the electrodes were further analyzed with UV–vis diffuse reflectance spectrometry in order to gain the knowledge on their optical properties. As shown in Fig. 4, the electrodes A and B have no distinct absorption (expressed as a Kubelka–Munk unit) in the range of $\lambda > 340$ nm.

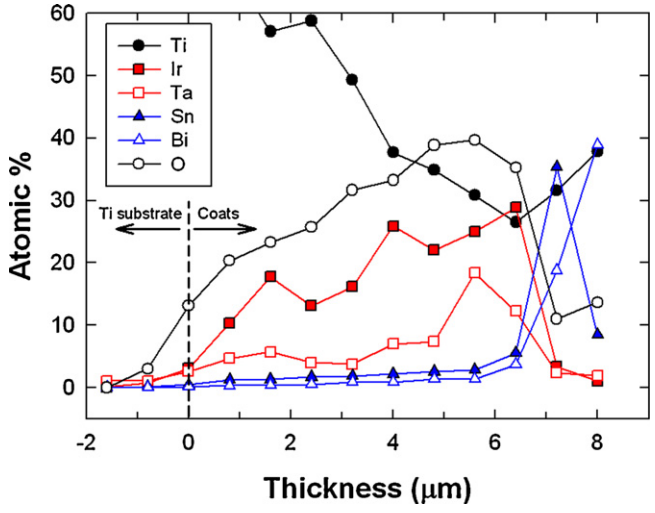

Fig. 2. Electron probe microanalysis of the BiO_x–TiO_2/Ti electrode (electrode C in Table 1).

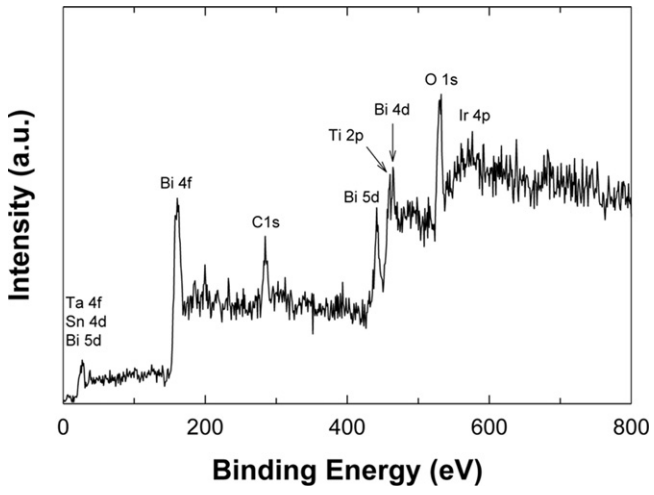

Fig. 3. X-ray photoelectron spectroscopy analysis of the BiO_x–TiO_2/Ti electrode (electrode C).

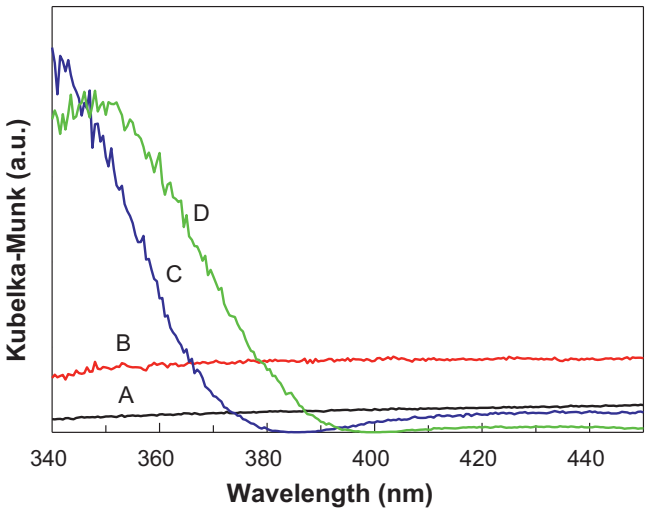

Fig. 4. UV–vis diffuse reflectance absorption spectra of electrode samples. The absorbances were recorded with respect to $BaSO_4$ pellet and expressed as a Kubelka–Munk unit.

Since IrO_x and TaO_x are non-light absorbing ceramics (electrode A) and the semiconducting SnO_2 (electrode B) can absorb light of wavelength shorter than ca. 326 nm due to its large bandgap of 3.8 eV ($\lambda = hc/E_g \cong 1240/3.8 = 326$ nm), such UV-transparent property is reasonable. Meanwhile, the electrodes C and D have a distinct UV light absorption from at 380 nm and 395 nm corresponding to bandgaps of ca. 3.26 and 3.14 eV, respectively. This light absorption property should be attributed to the presence of TiO_2 particles commonly found in both electrodes. In addition, the blue shift of electrode C as compared to that of electrode D might be attributed to the sodium present on the outermost surface. Such optical property of electrodes C and D, therefore, suggests that they can have photocatalytic or photoelectrocatalytic activity under the irradiation conditions of UV light.

3.2. Photoelectrocatalytic activity of electrodes

Before testing the two-electrode electrochemical cell, cyclic voltammograms of BiO_x–TiO_2 (electrode C) were measured in a NaCl electrolyte (~pH 5). These results are shown in Fig. 5a. In the absence of light (i.e., with specific reference to the electrocatalytic or inner surface conditions), BiO_x–TiO_2 yields no significant oxidation peak up to $1.2V_{SCE}$ on a forward scan, but a linear increase of the anodic current is observed. This current is most likely associated with the oxidation of Bi(III) to Bi(IV) ($Bi_2O_4 + 4H^+ + 2e^- \leftrightarrow 2BiO^+ + 2H_2O$; $E^\circ = 1.593V_{NHE@pH\,0} = 1.057V_{SCE@pH\,5}$), water oxidation to oxygen ($O_2 + 4H^+ + 4e^- \leftrightarrow 2H_2O$; $E^\circ = 1.23V_{NHE@pH\,0} = 0.694V_{SCE@pH\,5}$), and chloride oxidation ($Cl_2^- + e^- \leftrightarrow 2Cl^-$; $E^\circ = 1.76V_{SCE}$). On the other hand, the cathodic (reverse) scan generates two apparent peaks at ca. 0.9 and $0.4V_{SCE}$. The former is attributed to hypochlorous acid reduction ($HClO + H^+ + 2e^- \leftrightarrow Cl^- + H_2O$) occurring at $1.49V_{NHE@pH\,0}$ ($=0.95V_{SCE@pH\,5}$) while the latter is related to hypochlorite reduction ($ClO^- + H_2O + 2e^- \leftrightarrow Cl^- + 2OH^-$) occurring at $0.90V_{NHE@pH\,0}$ ($=0.36V_{SCE@pH\,5}$). Irradiation of the electrode with light at $\lambda > 320$ nm (i.e., on the photoelectrocatalytic or outer anode surface) increases the anodic current over the entire applied potential range indicating that more electrons are generated and directed through the circuit. These cyclic voltammograms are very similar to those with phenol as a model chemical contaminant in water (data not shown). It is noteworthy that the non-doped TiO_2 electrode (i.e., TiO_2/Ti) did not generate any measurable currents over the same applied potential range in the dark due to the absence

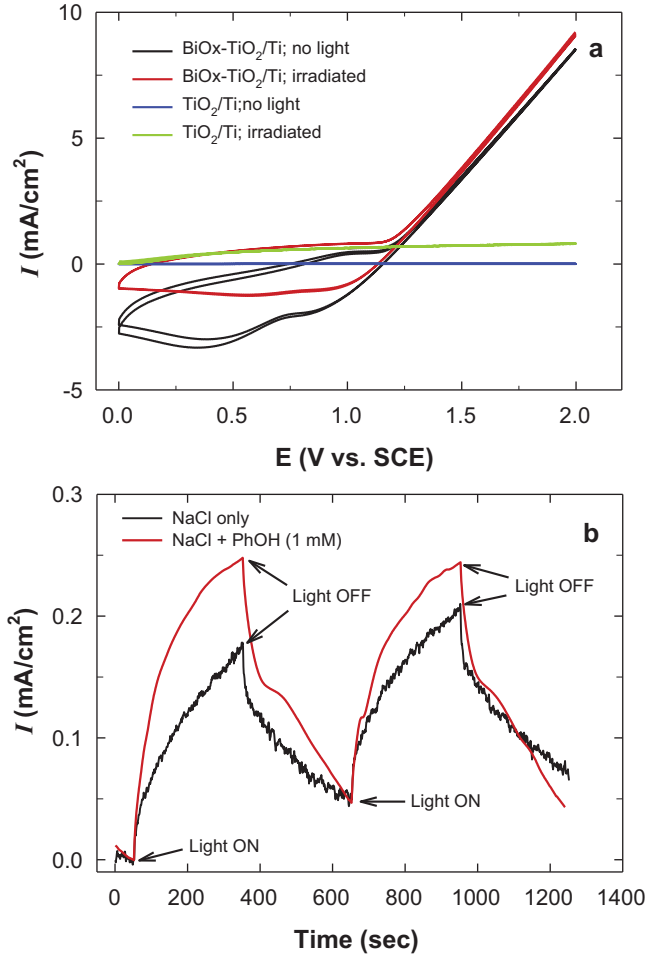

Fig. 5. (a) Cyclic voltammetries of the BiO_x–TiO_2/Ti electrode (electrode C) in 0.1 M NaCl electrolyte with or without AM 1.5 light irradiation. (b) Time profile of photocurrent generation at 1.3 V vs. SCE in the presence of 1 mM phenol in 0.1 M NaCl.

of electrocatalytic activity. The irradiation of TiO_2/Ti generated a moderate level of currents, yet its magnitude was much smaller than those of BiO_x–TiO_2/Ti electrode. Fig. 5b illustrates the photoenhancement effects in a more comparative way. In the absence of phenol (i.e., the electron donor), the output of the BiO_x–TiO_2 electrode is in the range of 1.7–2.0 mA/cm^2 at $1.3V_{SCE}$ after the light is turned on. With the addition of phenol to the electrolyte, the anodic photocurrent is increased by as much as 50%. This is a clear indication that the oxidation of phenol enhances the performance of the anode. This observed substrate-enhanced current generation shows that the electron–hole pairs are produced upon irradiation of the BiO_x–TiO_2 anode and that the recombination of the charge pairs is inhibited by the electron donor.

In order to investigate the effects of UV–vis irradiation to the BiO_x–TiO_2 anode coupled with the stainless steel cathode on the anodic oxidation of phenol and the concomitant cathodic H_2 production rate, a variation of the applied DC voltages was investigated. As shown in Fig. 6a, applications of irradiation only or irradiation with 1.0 V of cell voltage (E_{cell}) did not cause any degradation of phenol. Direct UV photolysis (i.e., without the BiO_x–TiO_2 anodes) also did not change the concentration of phenol (data not shown). It was found that overall operation of the fabricated cell begins at above 2.0 V (see Fig. 7), from where the concentration of phenol is decreased according to pseudo first-order kinetics ($-d[\text{phenol}]/dt = k_{obs}[\text{phenol}]$). It was also found that the cathodic hydrogen is produced rather linearly. The anodic and cathodic reactions are enhanced with increasing cell voltages. For

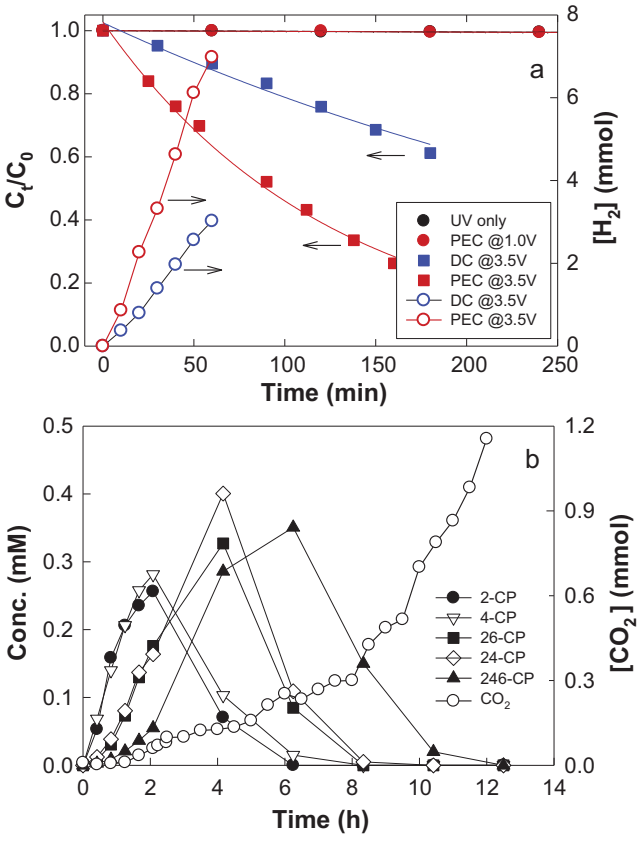

Fig. 6. (a) Time profiles of phenol degradation with the BiO_x–TiO_2/Ti electrode (electrode C) in 0.1 M NaCl electrolyte with or without UV light irradiation. $[Phenol]_0$ = 1 mM; [NaCl] = 50 mM (1.5 L); λ > 320 nm. (b) Time profiles of chlorinated phenols (CP) and CO_2 generated during the photoelectrochemical (PEC) oxidation of phenol at E_{cell} = 3.5 V; $[Phenol]_0$ = 1 mM; [NaCl] = 50 mM (1.5 L); λ > 320 nm. CP refers to chlorinated phenol.

example, at E_{cell} = 3.5 V, the degradation rate of phenol with light irradiation is three times higher than that without light, while the cathodic hydrogen production rate is over two times higher (Fig. 6a). It should be noted that the electrocatalytic oxidation of phenol resulted in the generation of diverse chlorinated phenols (mono-, di-, and tri-chlorophenols) by stepwise chlorination at initial phase but all the chlorinated intermediates were ultimately oxidized into carbon dioxide at prolonged electrolysis [10,38,39]. The photoelectrocatalytic degradation of phenol also has a similar set of intermediates (i.e., chlorinated phenols) with trace amounts of hydroxylated phenols (hydroquinone and catechol) at the initial phase (Fig. 6b). At the initial phase, monochlorinated phenols are generated, which are transformed into di- and trichlorinated phenols at the intermediate phase, and subsequently undergo the ring cleavage and oxidation to organic acids such as oxalic, maleic, and formic acids. Eventually, these daughter acids are further degraded at the electrode surface to aqueous carbon dioxide with the subsequent release of gaseous CO_2. At the stage of complete degradation of 2,4,6-trichlorophenol (12.5 h), ca. 1.2 mmol carbon was released indicating that ca. 13% of initial molar amount of carbon (1 mmol-phenol/L × 1.5 L × 6 carbons/phenol = 9 mmol carbon) was released as CO_2. This suggests that the remaining carbons may exist in the aqueous phase in the forms of ring-cleaved intermediates and inorganic carbons (e.g., CO_2, H_2O, HCO_3^-, CO_3^{2-}). Therefore, the photoelectrocatalytic degradation mechanism of phenol is very similar to the electrocatalytic mechanism despite much facilitated kinetics in the photoelectrocatalytic reaction.

Fig. 7 compares the electrocatalytic and photo-electrocatalytic effects quantitatively as a function of applied cell voltages. The

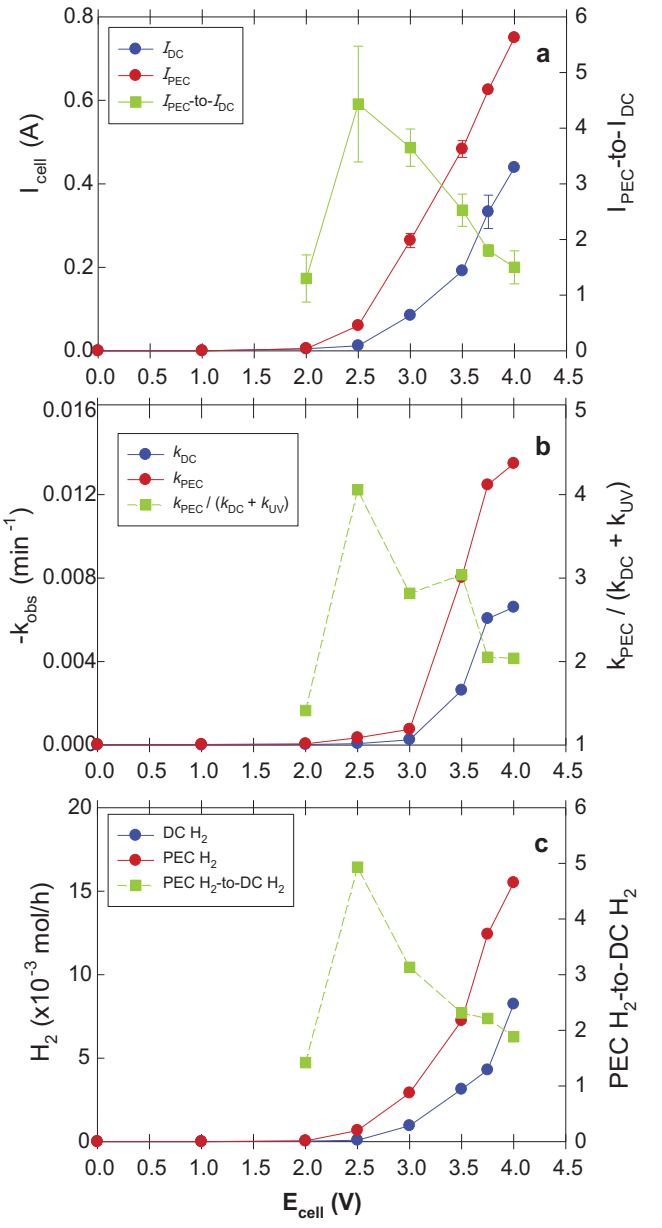

Fig. 7. Comparison of electroctatalytic and photoelectrocatalytic performances of BiO_x–TiO_2 anode (electrode C) and stainless steel couple as a function of applied DC voltages. (a) Cell current (I_{cell}) generations, (b) pseudo-first order reaction rate ($-k_{obs}$) of phenol (C_0 = 1 mM) and (c) cathodic hydrogen production rate.

electrocatalytic *I–V* curve is very similar to previous studies in that onset of a measureable current, I_{cell}, occurs close to 2.0 V and then increases exponentially as the potential is increased (Fig. 7a). Photoelectrocatalytic *I–V* curve shows a similar response although with a maximum four-fold enhancement of I_{cell}. This result provides evidence that the outer face also works in a similar fashion as the inner surface. UV–vis irradiation at λ > 320 nm of the anode enhances the rate of oxidative degradation of phenol (k_{obs}) by factors of 2–4 depending on the specific value of E_{cell} (Fig. 7b). Increases in I_{cell} show that more electrons are transported to the cathode and thus more H_2 should be produced as a result. Fig. 7c illustrates that the photoelectrochemical H_2 production rate is at least two-fold higher than the corresponding electrochemical rate in the absence of light. Furthermore, from the data presented in Fig. 7, it is evident that light irradiation to the outer face of the anode also increases the overall cell efficiency.

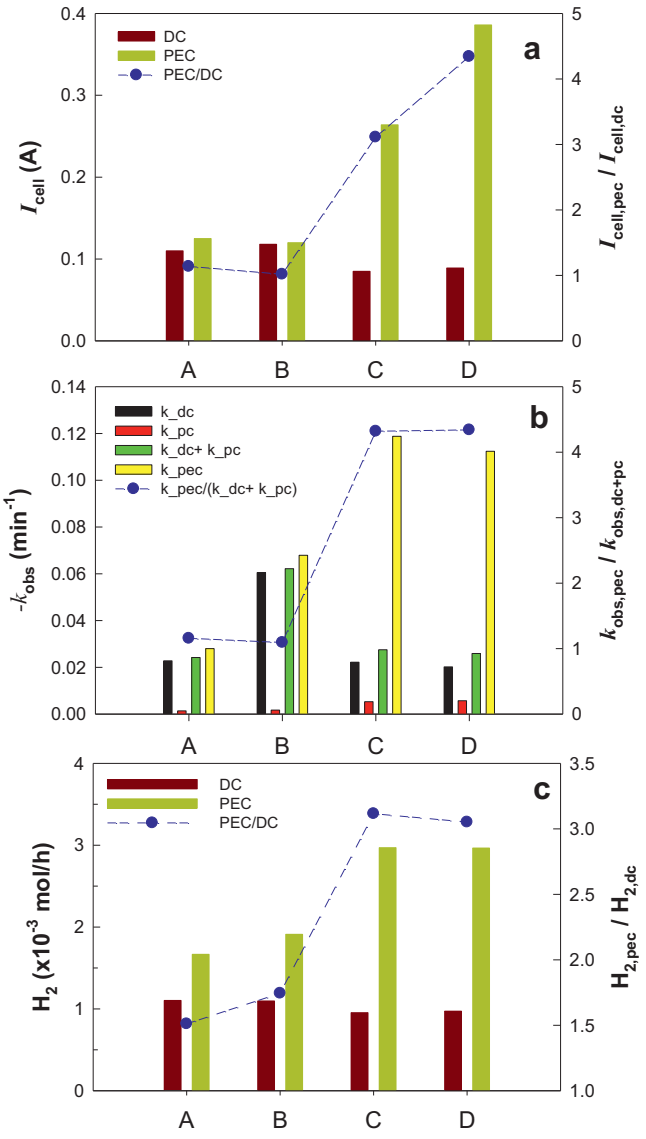

Fig. 8. Comparison of anodes for their electroctatalytic and photoelectrocatalytic performances of (a) cell current (I_{cell}) generations, (b) pseudo-first order reaction rate ($-k_{obs}$) of phenol, and (c) cathodic hydrogen production rate. E_{cell} = 3.00(±0.02) V; [Phenol]$_0$ = 1 mM; λ > 320 nm. Note that definition of "synergy" in Fig. 8a and c (synergy = PEC/(DC + light) is technically the same with that in Fig. 8b (synergy = PEC/DC) because the light irradiation generated neither cell current (I_{cell} in Fig. 8a) or hydrogen (Fig. 8c) (i.e., light effect = zero; hence PEC/(DC + light) = PEC/DC).

The four different anodes listed in Table 1 are compared for their electrocatalytic and photoelectrocatalytic performances in terms of I_{cell}, k_{obs} for phenol oxidation, and H_2 production rates. The experimental data is shown in Fig. 8 and summarized in Table 1. All four anodes, in principle, can be used as electrocatalysts for the treatment of chemical contaminants in water and for the oxidation of water to oxygen. For example, IrO_2 anode oxidizes water or water contaminants via Ir(IV/V) inter-valence state changes. BiO_x is likely to have a similar electrochemical behavior (Bi(III/IV) during the anodic treatment of water (Fig. 5). Thus, it is not surprising that electrodes A and B, which have no outer layer coating of BiO_x–TiO_2, exhibit higher DC currents and phenol degradation rates than C and D with BiO_x–TiO_2 since the IrO_2 (A) and SnO_2 (B) electrodes are proven to be effective for water treatment [3,9]. However, when exposed to light the BiO_x–TiO_2 electrodes generated higher cell currents than IrO_2 and SnO_2 electrodes, which correspond

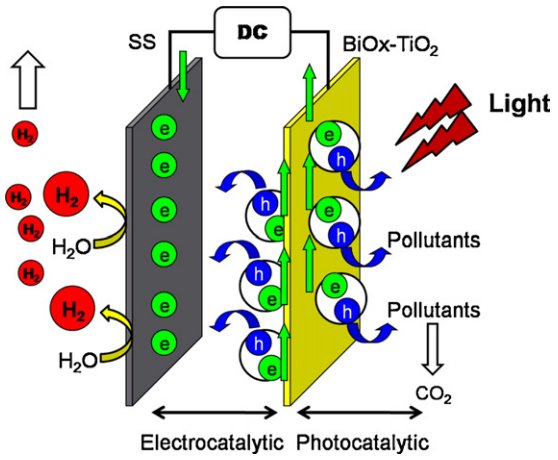

Scheme 1. Schematic illustration of a DC-powered (photo)electrochemical treatment of phenol contaminated water at BiO_x–TiO_2 anode with simultaneous hydrogen production from water at a stainless steel cathode. Note that the inner surface facing the cathode works as an electrocatalyst and the outer surface irradiated by UV-light works as a photoelectrocatalyst.

to a synergistic effect in the range of 300–430%. The apparent synergistic effect is more pronounced for the anodic oxidation of phenol where the rates are enhanced by factors of over 5 and 22 as compared to DC and UV, respectively. In the case of the cathodic production of H_2, the effects of the BiO_x–TiO_2 layer were slightly reduced with the H_2 current efficiencies in the range of 60–70%. The apparent synergistic effects for H_2 production are most likely due to the higher photocurrents. Overall, these results show that the BiO_x–TiO_2 coating serves as an effective anode, but also has a substantial potential as a photoanode.

3.3. BiO_x–TiO_2 electrodes with dual functionality

In Scheme 1, we illustrate the principal operative mechanism of the BiO_x–TiO_2 and SS couple under light irradiation. The inner face of the electrode functions as an electrocatalyst while the outer face is active as a photoelectrocatalyst. In the two-electrode setup, the anode surface not facing the cathode is assumed to have no electrocatalytic activity. In addition, since the Ti-foil base support is non-transparent to irradiated light, the inner face should be inactive with respect to photocatalysis. The control anodes with no surface coating of BiO_x–TiO_2 were also tested to investigate the role of BiO_x–TiO_2 in a quantitative way. Similar approaches of combining an electrocatalyst with a photoelectrocatalyst have been reported recently. For example, Drew et al. [43] reported on enhanced direct methanol fuel cell performance by employing a hybrid carbon fiber electrode consisting of a TiO_2 photocatalyst and Pt–Ru catalyst; UV-irradiation to the TiO_2 side of the electrode resulted in a 25% increase of the cell power density. In another application, Li et al. [44] inserted Sb–SnO_2 into TiO_2 nanotubes and found that the nanotubes increased the service life time of the electrocatalyst and enhanced the oxidative transformation of phenolic compounds to CO_2 and other inorganic products

It should be noted that the BiO_x–TiO_2 anode, which is employed in this study, is somewhat different from the conventional Bi-doped TiO_2 photocatalysts. For example, Bi-doped TiO_2 can be classified in several different ways. Three different Bi-doping types include: (1) Bi_2O_3–TiO_2 [45], (2) $Bi_xTi_yO_{1-x-y}$ which also functions as a photocatalyst [46], or as (3) Bi-doped TiO_2 which functions likewise as a visible-light photocatalyst [47]. The above materials were prepared with relatively small amounts of Bi (~1 mol%) with the primary purpose to develop new TiO_2 photocatalysts that

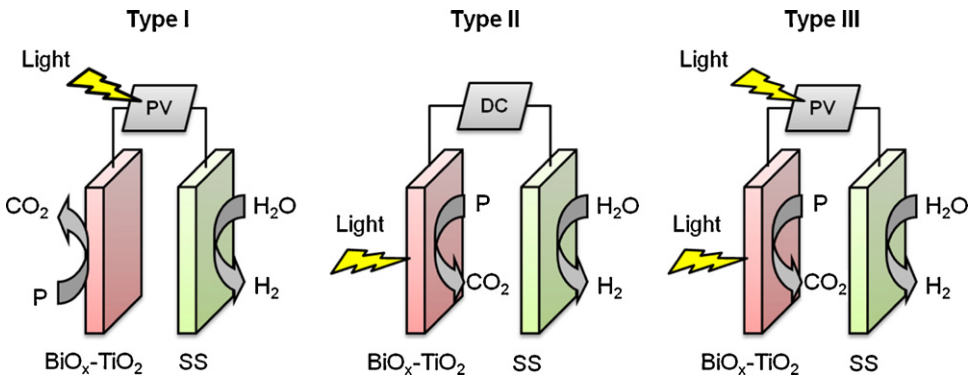

Scheme 2. Schematic illustration of three possible application types of BiO_x–TiO_2 electrode in electrolytic water treatment system and simultaneous hydrogen production from water. Type I: a photovoltaic (PV)-powered electrolysis, Type II: a DC-powered electrolysis with direct light irradiation to BiO_x–TiO_2 anode, Type III: a PV-powered electrolysis with direct light irradiation to BiO_x–TiO_2 anode. P: pollutants; SS: stainless steel cathode.

function under visible-light excitation (i.e., not functional without light). However, the BiO_x–TiO_2 of this study was prepared initially as an electrocatalyst intended specifically for water treatment applications. The Bi doping level of TiO_2 was designed to be as high as 25–33 mol% in the outermost electrode coat in order to increase conductivity. Thus, light irradiation to the BiO_x–TiO_2 without a DC power supply (i.e., no electrochemical bias) generates no measurable cell currents and or hydrogen. In the case of phenol oxidation, however, the BiO_x–TiO_2 particle arrays seem to have some photocatalytic activity toward phenol, and this activity is 3–4 times higher as those of the TaO_x–IrO_2 and BiO_x–SnO_2 electrodes (Table 1). Since the BiO_x–TiO_2 has a high extinction coefficient in the range of $\lambda < 395$ nm (Fig. 4), irradiation of the anode is likely in principle to create electron–hole pairs. However, most of excitons (electron–hole pairs) rapidly recombine in the absence of an external potential bias.

Scheme 2 illustrates three application types of the BiO_x–TiO_2 electrodes in water treatment and simultaneous hydrogen production from water. Type I is a PV-powered electrolysis and the BiO_x–TiO_2 electrode has been demonstrated to operate successfully due to its good electrocatatalytic property [10,38,39]. Type II is a DC-powered electrolysis with direct light irradiation to the BiO_x–TiO_2 electrode, which has been dealt with in this study. Finally type III is the combination of types I and II, i.e., a PV-powered electrolysis with light irradiation to the BiO_x–TiO_2 electrode. In this case, the PV arrays that significantly contributes to initial capital and operation/maintenance (O&M) cost in electrolytic water treatment system can be reduced in size by additional photoelectrocatalytic function of BiO_x–TiO_2. At present, we are testing the lab-scaled type III operation.

4. Conclusions

We have fabricated multi-layered BiO_x–TiO_2 electrocatalysts with heavy doping level of Bi and demonstrated that despite such doping they retained photoelectrocatalytic and electrocatalytic activities. Moreover, the BiO_x–TiO_2 electrocatalysts synergistically operated for degradation of phenol and hydrogen production in water under direct UV irradiation. The primary role of Bi doping is to increase TiO_2 conductivity, and to lend additional electrocatalytic properties via Bi(III/IV) inter-valence state changes during the electrocatalytic reactions. Most electrode-type electrochemical water treatment systems employ DC power as a primary operation energy source but this study suggests that diverse operation energy sources or their combination can be utilized when the BiO_x–TiO_2 electrodes are used as an anode.

Acknowledgements

This work was supported by the Basic Science Research Programs (No. 2009-0071350, No. 2009-0089904, and No. 2010-0002674) and the Korea Center for Artificial Photosynthesis (NRF-2009-C1AAA001-2009-0093879) through the National Research Foundation of Korea (NRF) funded by the MEST, Korea, and by the National Science Foundation (NSF Grant Number CHE-0924597) with additional support provided by the Northrop-Grumman Corporation.

References

[1] G.H. Chen, Electrochemical technologies in wastewater treatment, Sep. Purif. Technol. 38 (2004) 11–41.
[2] C.A. Martinez-Huitle, E. Brillas, Electrochemical alternatives for drinking water disinfection, Angew. Chem. Int. Ed. 48 (2008) 1998–2005.
[3] M. Panizza, G. Cerisola, Direct and mediated anodic oxidation of organic pollutants, Chem. Rev. 109 (2009) 6541–6569.
[4] S. Trasatti (Ed.), Electrodes of Conductive Metallic Oxides, Elsevier, New York, 1980.
[5] S. Ardizzone, G. Fregonara, S. Trasatti, Inner and outer active surface of RuO_2 electrodes, Electrochim. Acta 35 (1990) 263–267.
[6] O. Simond, V. Schaller, C. Comninellis, Theoretical model for the anodic oxidation of organics on metal oxide electrodes, Electrochim. Acta 42 (1997) 2009–2012.
[7] C. Borras, C. Berzoy, J. Mostany, J.C. Herrera, B.R. Scharifker, A comparison of the electrooxidation kinetics of p-methoxyphenol and p-nitrophenol on Sb-doped SnO_2 surfaces: concentration and temperature effects, Appl. Catal. B: Environ. 72 (2007) 98–104.
[8] J.M. Kesselman, O. Weres, N.S. Lewis, M.R. Hoffmann, Electrochemical production of hydroxyl radical at polycrystalline Nb-doped TiO_2 electrodes and estimation of the partitioning between hydroxyl radical and direct hole oxidation pathways, J. Phys. Chem. B 101 (1997) 2637–2643.
[9] S. Kim, S.K. Choi, B.Y. Yoon, S.K. Lim, H. Park, Effects of electrolyte on the electrocatalytic activities of RuO_2/Ti and Sb–SnO_2/Ti anodes for water treatment, Appl. Catal. B: Environ. 97 (2010) 134–141.
[10] H. Park, C.D. Vecitis, M.R. Hoffmann, Electrochemical water splitting coupled with organic compound oxidation: the role of active chlorine species, J. Phys. Chem. C 113 (2009) 7935–7945.
[11] P. Canizares, J.A. Dominguez, M.A. Rodrigo, J. Villasenor, J. Rodriguez, Effect of the current intensity in the electrochemical oxidation of aqueous phenol wastes at an activated carbon and steel anode, Ind. Eng. Chem. Res. 38 (1999) 3779–3785.
[12] P. Canizares, F. Martinez, M. Diaz, J. Garcia-Gomez, M.A. Rodrigo, Electrochemical oxidation of aqueous phenol wastes using active and nonactive electrodes, J. Electrochem. Soc. 149 (2002) D118–D124.
[13] C. Comninellis, A. Nerini, Aodic oxidation of phenol in the presence of NaCl for waste-water treatment, J. Appl. Electrochem. 25 (1995) 23–28.
[14] M. Panizza, C. Bocca, G. Cerisola, Electrochemical treatment of wastewater containing polyaromatic organic pollutants, Water Res. 34 (2000) 2601–2605.
[15] J. Iniesta, E. Exposito, J. Gonzalez-Garcia, V. Montiel, A. Aldaz, Electrochemical treatment of industrial wastewater containing phenols, J. Electrochem. Soc. 149 (2002) D57–D62.
[16] S. Tanaka, Y. Nakata, T. Kimura, M. Yustiawati, H. Kawasaki, Kuramitz, Electrochemical decomposition of bisphenol A using Pt/Ti and SnO_2/Ti anodes, J. Appl. Electrochem. 32 (2002) 197–201.

[17] X.Y. Li, Y.H. Cui, Y.J. Feng, Z.M. Xie, J.D. Gu, Reaction pathways and mechanisms of the electrochemical degradation of phenol on different electrodes, Water Res. 39 (2005) 1972–1981.
[18] B. Correa Lozano, C. Comninellis, A. De Battisti, Service life of $Ti/SnO_2–Sb_2O_5$ anodes, J. Appl. Electrochem. 27 (1997) 970–974.
[19] Y.J. Feng, X.Y. Li, Electro-catalytic oxidation of phenol on several metal-oxide electrodes in aqueous solution, Water Res. 37 (2003) 2399–2407.
[20] F. Montilla, E. Morallon, A. De Battisti, J.L. Vazquez, Preparation and characterization of antimony-doped tin dioxide electrodes. Part 1. Electrochemical characterization, J. Phys. Chem. B 108 (2004) 5036–5043.
[21] J. Iniesta, P.A. Michaud, M. Panizza, G. Cerisola, A. Aldaz, C. Comninellis, Electrochemical oxidation of phenol at boron-doped diamond electrode, Electrochim. Acta 46 (2001) 3573–3578.
[22] A. Morao, A. Lopes, M.T.P. de Amorim, I.C. Goncalves, Degradation of mixtures of phenols using boron doped diamond electrodes for wastewater treatment, Electrochim. Acta 49 (2004) 1587–1595.
[23] F. Bonfatti, S. Ferro, F. Lavezzo, M. Malacarne, G. Lodi, A.D. Battisti, Electrochemical incineration of glucose as a model organic substrate, J. Electrochem. Soc. 147 (2000) 592–596.
[24] C.P. De Pauli, S. Trasatti, Composite materials for electrocatalysis of O_2 evolution: $IrO_2 + SnO_2$ in acid solution, J. Electroanal. Chem. 538 (2002) 145–151.
[25] M. Li, C.P. Feng, W.W. Hu, Z.Y. Zhang, N. Sugiura, Electrochemical degradation of phenol using electrodes of $Ti/RuO_2–Pt$ and $Ti/IrO_2–Pt$, J. Hazard. Mater. 162 (2009) 455–462.
[26] N.B. Tahar, A. Savall, Mechanistic aspects of phenol electrochemical degradation by oxidation on a Ta/PbO_2 anode, J. Electrochem. Soc. 145 (1998) 3427–3434.
[27] Y.Z. Li, W. Xie, X.L. Hu, G.F. Shen, X. Zhou, Y. Xiang, X.J. Zhao, P.F. Fang, Comparison of dye photodegradation and its coupling with light-to-electricity conversion over TiO_2 and ZnO, Langmuir 26 (2010) 591–597.
[28] K. Vinodgopal, I. Bedja, P.V. Kamat, Nanostructured semiconductor films for photocatalysis. Photoelectrochemical behavior of SnO_2/TiO_2 composite systems and its role in photocatalytic degradation of a textile azo dye, Chem. Mater. 8 (1996) 2180–2187.
[29] Z.H. Zhang, M.F. Hossain, T. Takahashi, Self-assembled hematite (alpha-Fe_2O_3) nanotube arrays for photoelectrocatalytic degradation of azo dye under simulated solar light irradiation, Appl. Catal. B: Environ. 95 (2010) 423–429.
[30] Y.H. Ng, A. Iwase, A. Kudo, R. Amal, Reducing graphene oxide on a visible-light $BiVO_4$ photocatalyst for an enhanced photoelectrochemical water splitting, J. Phys. Chem. Lett. 1 (2010) 2607–2612.
[31] G. Waldner, A. Bruger, N.S. Gaikwad, M. Neumann-Spallart, WO_3 thin films for photoelectrochemical purification of water, Chemosphere 67 (2007) 779–784.
[32] H. Park, W. Choi, Photoelectrochemical investigation on electron transfer mediating behaviors of polyoxometalate in UV-illuminated suspensions of TiO_2 and Pt/TiO_2, J. Phys. Chem. B 107 (2003) 3885–3890.
[33] H. Park, W. Choi, Effects of TiO_2 surface fluorination on photocatalytic reactions and photoelectrochemical behaviors, J. Phys. Chem. B 108 (2004) 4086–4093.
[34] J.M. Kesselman, N.S. Lewis, M.R. Hoffmann, Photoelectrochemical degradation of 4-chlorocatechol at TiO_2 electrodes: comparison between sorption and photoreactivity, Environ. Sci. Technol. 31 (1997) 2298–2302.
[35] N. Strataki, V. Bekiari, D.I. Kondarides, P. Lianos, Hydrogen production by photocatalytic alcohol reforming employing highly efficient nanocrystalline titania films, Appl. Catal. B 77 (2007) 184–189.
[36] Y. Liu, B. Zhou, J. Bai, J. Li, J. Zhang, Q. Zheng, X. Zhu, W. Cai, Efficient photochemical water splitting and organic pollutant degradation by highly ordered TiO_2 nanopore arrays, Appl. Catal. B 89 (2009) 142–148.
[37] M. Catanho, G.R.P. Malpass, A.J. Motheo, Photoelectrochemical treatment of the dye reactive red 198 using DSA((R)) electrodes, Appl. Catal. B 62 (2006) 193–200.
[38] H. Park, C.D. Vecitis, W. Choi, O. Weres, M.R. Hoffmann, Solar-powered production of molecular hydrogen from water, J. Phys. Chem. C 112 (2008) 885–889.
[39] H. Park, C.D. Vecitis, M.R. Hoffmann, Solar-powered electrochemical oxidation of organic compounds coupled with the cathodic production of molecular hydrogen, J. Phys. Chem. A 112 (2008) 7616–7626.
[40] S. Murugesan, Y.R. Smith, V. Subramanian, Hydrothermal synthesis of $Bi_{12}TiO_{20}$ nanostrucutures using anodized TiO_2 nanotubes and its application in photovoltaics, J. Phys. Chem. Lett. 1 (2010) 1631–1636.
[41] U.A. Joshi, A. Palasyuk, D. Arney, P.A. Maggard, Semiconducting oxides to facilitate the conversion of solar energy to chemical fuels, J. Phys. Chem. Lett. 1 (2010) 2719–2726.
[42] O. Weres, Electrode with surface comprising oxides of titanium and bismuth and water purification process using this electrode, US Patent 7,494,583 B2, 2009.
[43] K. Drew, G. Girishkumar, K. Vinodgopal, P.V. Kamat, Boosting fuel cell performance with a semiconductor photocatalyst: TiO_2/Pt–Ru hybrid catalyst for methanol oxidation, J. Phys. Chem. B 109 (2005) 11851–11857.
[44] P.Q. Li, G.H. Zhao, X. Cui, Y.G. Zhang, Y.T. Tang, Constructing stake structured TiO_2-NTs/Sb-doped SnO_2 electrode simultaneously with high electrocatalytic and photocatalytic performance for complete mineralization of refractory aromatic acid, J. Phys. Chem. C 113 (2009) 2375–2383.
[45] S. Shamaila, A.K.L. Sajjad, F. Chen, J.L. Zhang, Study on highly visible light active Bi_2O_3 loaded ordered mesoporous titania, Appl. Catal. B: Environ. 94 (2010) 272–280.
[46] W.F. Yao, X.H. Xu, H. Wang, J.T. Zhou, X.N. Yang, Y. Zhang, S.X. Shang, B.B. Huang, Photocatalytic property of perovskite bismuth titanate, Appl. Catal. B: Environ. 52 (2004) 109–116.
[47] Y.Q. Wu, G.X. Lu, S.B. Li, The doping effect of Bi on TiO_2 for photocatalytic hydrogen generation and photodecolorization of Rhodamine B, J. Phys. Chem. C 113 (2009) 9950–9955.